frontiers | Frontiers in Materials

TYPE Original Research
PUBLISHED 20 December 2023
DOI 10.3389/fmats.2023.1322898

OPEN ACCESS

EDITED BY
Martin I. Pech-Canul,
Centro de Investigación y de Estudios Avanzados Unidad Saltillo, Mexico

REVIEWED BY
Rodrigo Moreno,
Spanish National Research Council (CSIC), Spain
Adriano Michael Bernardin,
University of the Extreme South of Santa Catarina, Brazil

*CORRESPONDENCE
Edén A. Rodríguez,
eden.rodriguezcs@uanl.edu.mx,
earc22@hotmail.com

RECEIVED 17 October 2023
ACCEPTED 05 December 2023
PUBLISHED 20 December 2023

CITATION
Rodríguez EA, Díaz-Tato L, López-Perales JF and González-Carranza Y (2023), Effect of binary raw materials replacement (quartz and feldspar) for porcelain chamotte on the electro-technical siliceous porcelain properties.
Front. Mater. 10:1322898.
doi: 10.3389/fmats.2023.1322898

Effect of binary raw materials replacement (quartz and feldspar) for porcelain chamotte on the electro-technical siliceous porcelain properties

Edén A. Rodríguez*, Leonel Díaz-Tato, J. F. López-Perales and Yadira González-Carranza

Facultad de Ingeniería Mecánica y Eléctrica (FIME), Programa Doctoral en Ingeniería de Materiales, Universidad Autónoma de Nuevo León (UANL), San Nicolás de los Garza, Nuevo León, México

The hurry for ecological practices and waste control has emerged as an obligation in modern times, demanding precise strategies to restrain waste accumulation and to stimulate recycling and reuse actions to lower the climate effect. The replacement of binary raw materials for porcelain chamotte waste in siliceous porcelain was studied to obtain eco-friendly high-voltage porcelain. Quartz and feldspar were progressively replaced by 5, 10, and 15 wt.% of porcelain chamotte in a conventional siliceous electro-technical porcelain composition. The replacement effect on sintered samples at 1250°C under industrial heat treatment was evaluated by measuring the linear shrinkage, bulk density, porosity, flexural strength, and microhardness technological properties. Phase analysis was carried out by X-ray diffraction. Microstructural characteristics were studied using a scanning electron microscope. The results showed that chamotte-containing samples reached bulk densities of about 2.36 g/cm^3 and a porosity percentage near zero. The maximum flexural strength value at glazed states was 87.8 MPa, for 15 wt.% scrap-containing samples. X-ray diffraction studies revealed a higher mullite phase content in chamotte-containing samples. Scanning electronic microscopy images of the polished and etched specimens show the presence of quartz grains and secondary mullite needles embedded in a feldspathic vitreous matrix. The properties reached by the chamotte-containing samples are attractive since the values obtained in terms of flexural strength, density, and porosity are compared to those reported for conventional siliceous porcelain were obtained. The most noticeable result was observed in flexural resistance. The glazed porcelain bodies showed a flexural strength improvement of about 15%. Then, these porcelain compositions suggest an alternative to produce a more sustainable, affordable, and environmentally-friendly porcelain insulator product.

KEYWORDS

electro-technical porcelain, chamotte, microstructure, mechanical properties, sustainable material, replacement

1 Introduction

New regulations and "green" actions focusing on environmental issues provoked by the ascending tendency of industrial waste generation are demanded worldwide (Quaranta et al., 1998; Benavidez et al., 1999; Sepehri and Sarrafzadeh, 2018; Gharibi et al., 2022). The hurry for ecological practices and waste control has emerged as an obligation in modern times, demanding precise strategies to restrain waste accumulation and to stimulate recycling and reuse actions to lower the climate effect (Penteado et al., 2016; Nodeh, 2017; Lassinantti Gualtieri et al., 2018; Sepehri and Sarrafzadeh, 2018; Owoeye et al., 2019; Naenudon et al., 2023).

A few years ago, the economy operated following a linear "collection, production, and disposal" model, where all products would undoubtedly reach an "end-of-life" state (Almeida et al., 2016). Nevertheless, one of the concepts that currently seems to be booming worldwide is the circular economy. It has recently emerged as an innovative industrial concept based on resource optimization and waste reduction. The transition towards a circular economy can be the biggest revolution in manufacturing and consumption in the global economy for the next future (Geissdoerfer et al., 2017; García-Muiña et al., 2018; Marvila et al., 2021).

In this context, ceramic manufacturing produces an enormous waste volume, which might reach ⅓ of the overall industrial ceramic manufacture (Tikul, 2014; Awoyera et al., 2016; Khan et al., 2016; Belhouchet et al., 2019). Most waste cannot be recycled back into the production process in the plants. Thus, they are inevitably disposed of as industrial waste, affecting the environment (Kelestemur et al., 2014; Mohamed et al., 2014; Xu et al., 2015; Khan et al., 2016; Mohammad et al., 2016; Tam et al., 2018). Indeed, it is estimated that at least 10% of the total industrial ceramics manufacture stands for industrial waste generated from the same process.

Furthermore, the ceramic industry is considered a heavy industry that consumes large amounts of mineral resources, such as high-quality sources of feldspar and quartz. These minerals and others have been increasingly depleted to the point of becoming exhausted (Marvila et al., 2021; Ogbonda and Onuchuku, 2021; Altimari et al., 2023). As a result, the ceramic industry already includes by-product recycling practices. It is well known that clay-based ceramic products, including porcelain, are suitable recycling systems for incorporating many types of industrial waste (Conte et al., 2020; Locks et al., 2021; Addis et al., 2023).

From 1850 until now, porcelain has been the dominant insulators material used for the power system industry (Liebermann, 2000; Amigó et al., 2005; Gubanski, 2010; Meng et al., 2012; Contreras and Rodriguez, 2017; Ogbonda and Onuchuku, 2021; Addis et al., 2023). The accelerated power industry expansion has led to a worldwide demand for electrical insulators (Alhumoud, 2005; Ren et al., 2014; Al-Gheilani et al., 2017; Cicek et al., 2018; Merga et al., 2019). The typical composition of siliceous porcelain insulators consists of 40%–50% clay, 10%–15% quartz, and 35%–45% feldspar (all percentages by weight) (Harper, 2001; Braganca and Bergman, 2004; Dana et al., 2004; Sánchez et al., 2010; Liebermann, 2012; Piva et al., 2016; Owoeye et al., 2019). Among the materials that constitute electrical porcelain, feldspar is a high-cost raw material. Besides, the resources of high-grade feldspar minerals and deposits of high-quality quartz sands have recently begun to be depleted (Addis et al., 2023).

On the other hand, innumerable refused electro-technical porcelain insulators by quality control parameters during their manufacture, and some insulators whose lifetime concluded have been turned into ceramics waste, nearly all of which were not reprocessed or recycled. The total amount of electro-technical insulator waste grows by massive tons every year. This occurrence provokes alarming environmental contamination (Suttibak and Nitivattananon, 2008; Xie et al., 2012; Cregut et al., 2013; Sanyal et al., 2020; Pereira et al., 2022). Therefore, the disposal of electro-technical porcelain insulators has become a critical issue in many nations (Brito and Saikia, 2013; Xu et al., 2015; Khan et al., 2016; Cicek et al., 2018; Tam et al., 2018). Lately, so much interest has been placed in siliceous electro-technical porcelain that does not meet the quality requirements necessary to be sold as a reliable electrical insulator, ending up as a discarded product, i.e., as an industrial by-product known as chamotte (Khan et al., 2016; Meng et al., 2016). Since chamotte was subjected to the typical sintering process to produce an electrical insulator, it will offer stable physical and chemical characteristics to be incorporated into ceramic bodies (Belhouchet et al., 2019).

Sustainable waste management is based on reduction, reuse, and recovery in descending order of priority. The use of industrial waste in the manufacture of electro-technical porcelain achieves all these objectives simultaneously since it not only solves the waste disposal by the companies that generate it but also reduces the consumption of raw materials and energy, with the consequent saving of resources (Almeida et al., 2016).

Given the above, the use of chamotte as an alternative material (by-product) in electro-technical porcelain manufacture might provide advantages in mechanical, physical, or chemical properties over the conventional ones in addition to reducing costs related to the extraction and transportation of raw materials and preventing environmental degradation by transforming what was considered waste into a valuable resource (García-Muiña et al., 2018; Marvila et al., 2020; Locks et al., 2021).

Few studies on porcelain insulators using chamotte in their chemical composition have been published (Gress and Leshchenko, 1967; Caligaris et al., 2000; Fassbinder, 2002; Liu et al., 2019). The early porcelain chamotte addition in high-voltage insulator manufacture was reported by R. I. Gress and N. P. Leshchenko (Gress and Leshchenko, 1967). They concluded that the most attractive formulation was constituted by 26% porcelain chamotte, which satisfied the electrical insulating basic requirements besides a higher mechanical strength by virtue of the higher alumina (Al_2O_3) content. Gunter Fassbinder studied ground scrap from sintered insulators into alumina porcelain insulators. Coarse ground scrap was added as a raw material to accomplish resistance demands and overcome surface imperfections over the forming stage for insulator production. The conclusion indicated that more scrap (chamotte) helps to reach higher mechanical strength (Fassbinder, 2002). The effect of using porcelain chamotte from insulator production was explored by Caligaris et al. The main finding showed that the porcelain chamotte addition improves the strength of sintered porcelain bodies (1250°C to 1300°C) thanks to a higher concentration of mullite phase (Caligaris et al., 2000).

In a previous study, the substitution of quartz by fired electrical porcelain scrap in a siliceous porcelain insulator was reported. The

substitution of 5 wt.% of SiO_2 (quartz) with chamotte in the siliceous porcelain led to a flexural strength improvement of 7% in porcelain bodies without glaze. Meanwhile, this same 5 wt.% of SiO_2 substitution with chamotte in the siliceous porcelain resulted in a flexural strength improvement of 15% in glazed porcelain bodies (Rodriguez et al., 2019).

Nevertheless, the study of the feldspar raw material's substation by industrial waste is of paramount importance since it is regarded with the formation of the glassy phase that allows the open pores present in the microstructure to be filled by capillary action and contributes to the formation of the mullite phase required in the ceramic body. Previous studies have identified various silica-based wastes with the potential to partially replace feldspar, among the most reported being glass waste. However, although benefits in terms of cost reduction by improving the alkali content and reducing the firing temperature are obtained, effects such as permanent deformations and extent to the initial densification stage have also been identified, causing a lower sintering efficiency (Conte et al., 2020; Addis et al., 2023; Altimari et al., 2023).

On the other hand, it is known that the properties exhibited by porcelain insulators, such as mechanical resistance and dielectric strength, could be affected by the development of phases present in the microstructure, which are a function of the quality and quantity of the used raw materials. Mullite and glassy phases are the main phases influencing these properties, so an excessive amount of glassy phase promotes the free movement of ions in the porcelain body, resulting in poor electrical insulation (Merga et al., 2019; Sanyal et al., 2020).

Considering the above discussed, this investigation introduces a circular economy approach related to the binary raw materials replacement for porcelain chamotte in siliceous porcelain. The current research aims to evaluate the effect of a binary traditional raw materials substitution (quartz and feldspar) for porcelain chamotte in siliceous electro-technical porcelain to obtain eco-friendly high-voltage porcelain insulators.

2 Experimental procedure

2.1 Materials

There were two kinds of raw material used in this research which are listed as follows with their respective mean particle size (all raw materials have a multimodal particle size): i) traditional raw materials-kaolin, (d_{50} = 11.43 μm); feldspar, (d_{50} = 21.24 μm); clay, (d_{50} = 1.60 μm), and quartz, (d_{50} = 21.74 μm). ii) by-product material-porcelain chamotte, (d_{50} = 13.66 μm). The kaolin, quartz, and feldspar were provided by Covia, Nuevo Leon, Mexico. Meanwhile, the K-blend was provided by Imerys Ceramics Mexico (KT clay), Nuevo Leon, Mexico. The particle size distribution of the raw materials was determined using the laser diffraction granulometry method (HORIBA laser model LA-950, Jobin Yvon R&D, Kyoto, Japan).

The raw materials' chemical composition was evaluated employing an X-ray fluorescence spectrometer (XRF, Philips PW 2400 model, Eindhoven, Netherlands). For XRF analysis, the sample (10 g) must be prepared to reach uniform particle size distribution and density through a milling process for 2 min in a mixer mill. Once the sample has been sufficiently homogeneous, it can be pressed into a tablet. Often, the tablet is only mechanically stable if a binding agent is added (acetylsalicylic acid) to it. To completely evacuate the air from the sample, a pressure of 20 tons is used to reach maximum density. The raw materials' phase constitution was determined by a Bruker D8 Advance X-ray diffractometer (D8, Advance Bruker XRD diffractometer, Germany) with a Cu-Kα anode (λ = 0.1542 nm) operating at 45 KV and 40 mA. The diffraction patterns were collected at 25°C and over an angular range of $5^\circ \leq 2\theta \leq 90^\circ$ with a step size of 0.05° per step and a dwell time of 12 s per increment. The chemical composition resolved by XRF is shown in Table 1. The traditional material's XRD results are also shown in Table 1.

2.2 Experimental design and samples preparation

Four formulations were designed to study the chamotte effect on electro-technical porcelain insulator properties, where chamotte partially substituted quartz and feldspar as an alternative raw material in the conventional formulation. The control formulation (CSP) is a typical electro-technical siliceous porcelain without chamotte addition. In the remaining experimental formulation (CHP-1 to CHP-3 formulations), a weight percentage of quartz (SiO_2) and feldspar were gradually substituted by porcelain chamotte (5, 10, and 15 wt.%, correspondingly). The starting raw materials fractions of the four proposed experimental formulations are listed in Table 1.

Exploratory specimens were elaborated following a factory-made process for ordinary porcelain insulator fabrication. Raw materials lots (see portions provided in Table 1), osmosis water (40% of the total raw material weight with a pH ~6), and deflocculating additives (sodium silicate- 0.01wt.%) were homogenized in a mixer machine at a speed setting of 1200 rpm for 1.5 h. The porcelain barbotine (υ = 20 Pa s and $\rho = 1.62 \pm 0.02$ g/cm^3) was then pressed using a filter press to form a paste with suitable consistency (penetrometer index = 0.3–0.55 kg/cm^2) to be shape-formed in extruder equipment (6 kgf/cm^2 (0.58 MPa) of pressure and a contra pressure of 41.36 MPa). Extruded specimens with a geometry of 28.5 mm in diameter × 200 mm in length were manufactured and then stored at room temperature for 1 day. Afterward, the specimens were dried at 100°C ± 5°C in an industrial oven for 24 h. After the drying process, a lot was subjected to glazing by immersion. Finally, all specimens were sintered inside a stationary kiln using an industrial firing schedule (from a local porcelain insulator producer) at a soaking temperature of 1250°C (at least for ~ 2 h) and furnace-cooled to room temperature. The entire firing process lasts 32 h.

2.3 Methods

Sintered specimens were characterized for physical properties (bulk density, apparent porosity, and water absorption), thermal properties represented by dilatometry behavior, phase composition, microstructural features, mechanical behavior (modulus of rupture), and Vickers hardness.

The bulk density, water absorption, and apparent porosity's physical properties were calculated using Archimedes' Principle

TABLE 1 Chemical and phase compositions of raw materials by XRF and XRD analysis, experimental formulations design, physical properties of sintered samples, and chemical composition by XRF technique of sintered samples.

Raw materials	Oxide compounds (wt.%)												
	SiO_2	Al_2O_3	TiO_2	Fe_2O_3	CaO	MgO	K_2O	Na_2O	P_2O_5	ZrO_2	SrO	WO_3	Others/LOI
Chamotte	64.79	20.79	0.72	0.75	0.38	0.53	1.82	8.54	0.10	0.16	-	0.38	1.04
Kaolin	44.92	37.15	1.48	0.57	0.57	0.27	0.16	-	-	-	-	-	14.88
Feldspar	62.69	18.86	-	0.27	0.79	-	4.29	12.56	-	-	-	-	0.54
Clay	53.95	27.22	-	1.49	0.24	0.52	0.64	0.31	-	-	-	-	15.63
Quartz	95.41	1.50	-	0.08	0.22	-	0.26	0.13	-	-	0.38	-	2.02

Raw materials	**Phase composition**
Chamotte	Quartz (card number COD 00-900-9666); mullite (card number COD 00-900-5502)
Kaolin	Kaolinite (card number COD 00-900-9234)
Feldspar	Albite (card number COD 00-900-0681); Anorthoclase (card number COD 00-900-0860)
Clay	Kaolinite (card number COD 00-900-9234); Quartz (card number COD 00-153-6389)
Quartz	Quartz (card number COD 00-900-9666)

Formulations Design	Raw materials (wt.%)					Physical properties of sintered samples		
	Quartz	Feldspar	Clay	Kaolin	Chamotte	Bulk density (gr/cm^3)	Open porosity (%)	Water absorption (%)
CSP	26.8	26	30	17.2	0	2.27	<0.01	<0.01
CHP-1	24.3	23.5	30	17.2	5	2.35	<0.01	<0.01
CHP-2	21.8	21	30	17.2	10	2.35	<0.01	<0.01
CHP-3	19.3	18.5	30	17.2	15	2.38	<0.01	<0.01

Sintered samples	Oxide Compounds (wt.%)								
	SiO_2	Al_2O_3	TiO_2	Fe_2O_3	CaO	MgO	K_2O	Na_2O	LOI
CSP	66.99	20.045	0.647	0.745	0.428	0.382	1.863	8.334	0.161
CHP-1	66.38	22.29	0.69	0.83	0.28	0.30	2.11	7.01	-
CHP-2	65.36	22.29	0.52	0.83	0.22	0.35	1.65	8.73	0.05
CHP-3	65.62	22.77	0.64	0.81	0.26	-	1.75	8.02	0.13

10.3389/fmats.2023.1322898

following the boiling water method according to the ASTM C-20 Standard.

Crystalline phase analysis of sintered specimens was carried out by a Bruker D8 Advance X-Ray diffractometer (D8, Advance Bruker XRD diffractometer, Germany) with a Cu-Kα anode (λ = 0.1542 nm) operating at 45 KV and 40 mA. The diffraction patterns were collected at 25°C and over an angular range of 5°≤2θ ≤ 90° with a step size of 0.05° per step and a dwell time of 12 s per increment.

The structure at a micrometric scale of a representative sintered porcelain specimen of each formulation was analyzed by a Nikon Epiphot optical microscope (OM; Nikon Epiphot 200, Nikon Opticals, Tokyo, Japan). The obtained images were examined using a Clemex Vision PE Basics image analyzer. Also, the microstructure was analyzed, employing an FEI NOVA NANOSEM 200 SEM scanning electron microscope (FEI Company, Hillsboro, Oregon United States).

For qualitative and quantitative microanalysis, an Apollo XP detector was used (EDAX Apollo XP Silicon Drift Detector).

The modulus of rupture (flexural strength) on sintered specimens was tested using a Dillon-H35 hydraulic press machine (Dillon Dyno's Dynamometers, Liberty, MO, United States), following the IEC 60672 Standard. The loading rate suggested in standards is normally restricted to achieve fracture in 10 to 15 s. Crosshead speeds of 0.5 mm/min or loading rates of 50 N/s were used to achieve this target. The experimental cylindrical specimens have a geometry of 25.4 mm in diameter × 200 mm in length. 10 different measurements for each formulation were carried out, taking the average as the final reported values. Also, an analysis of variance (Tukey statistical test) was included in the mechanical properties results.

The microhardness was measured by the Vickers method. A Shimadzu HMV microhardness tester (Shimadzu HMV-2, Tokyo, Japan) was used. Polished sintered samples with dimensions 25.4 mm in diameter x 25.4 mm in height were tested. The final given values are the numerical mean of 15 evaluations on the surface for each experimental formulation. A 9.807 N loading force maintained for 15 s was used during the microhardness testing. Also, an analysis of variance (Tukey statistical test) was included in the mechanical properties results.

The thermic response of experimental samples (from room temperature to 1250°C) was studied by the thermal expansion coefficient calculation using a dilatometry technique. The analysis was performed by an MCC-01 463Harrop dilatometer (Harrop's Inc, Columbus, OH, United States), according to the IEC 672-2 standard. 47 mm was the original dimension in length of the specimens. 5°C per minute was used as the heating rate, and a soaking temperature was set at 1250°C, followed by a rapid cooling. The thermal expansion coefficient was calculated by the IEC 672-3 standard.

3 Results and discussion

3.1 Chamotte characterization

Figure 1 shows the chamotte XRD results, and its particle size distribution measured by the laser diffraction granulometry method (HORIBA laser model LA-950). From the particle size analysis, it is possible to observe that the mean particle size (d_{50}) of the chamotte waste (d_{50} = 13.66 μm) is smaller than that of the traditional raw materials that it partially replaces (quartz-d_{50} = 21.74 μm and feldspar-d_{50} = 21.24 μm). This characteristic can be beneficial since the particle size distribution significantly influences the packing of the particles and the sintered product. Therefore, the smaller size of chamotte waste particles can lead to greater surface areas, favoring the reaction kinetics between them and the diffusion process during phase transformation (Figueirêdo et al., 2020; Almeida et al., 2021).

According to the XRD analysis, $Al_6Si_2O_{13}$ (mullite, card number COD 00-710-5502) and SiO_2 (quartz, card number COD 00-900-9666) were the primary phases identified in the by-product material-porcelain chamotte. Meanwhile, SiO_2 and Al_2O_3 were the primary oxides in the by-product material (porcelain chamotte) detected by XRF analysis.

3.2 Physical properties

Table 1 summarizes the density, porosity, and water absorption results. An increasing density tendency is observed as chamotte is added to the CSP formulation (control formulation). This observance might be associated with a higher mullite content originating from the porcelain chamotte due to a higher mullite density (3.2 g/cm^3) than the other components of the porcelain matrix (quartz-2.6 g/cm^3, feldspar-2.56 g/cm^3, kaolinite-2.65 g/cm^3) (Xie et al., 2012; Harabi et al., 2017; Mehta et al., 2018).

Meanwhile, open porosity and water absorption do not suffer any modification by the chamotte adding. Water absorption and open porosity values are below 0.01%. These registered values are essential for electrical insulating applications to improve humidity resistance and avoid flashover voltage (Mehta et al., 2018; Owoeye et al., 2019; Ahmed Salem et al., 2022).

3.3 Phase mineralogical evolution

Figure 2 shows the contrast between X-ray diffraction patterns of the sintered formulations studied in this research. The crystalline phase study shows that SiO_2 (card number COD 00-900-9666) and $Al_6Si_2O_{13}$ (card number COD 00-710-5502), i.e., quartz and mullite, are the major phases that conforms the matrix. Also, the halo associated with the amorphous/glassy phase is observed. The vitreous phase concentration remains almost unmodified as chamotte is added (a slight increment can be detected). Chamotte addition might increase the amorphous phase in the porcelain matrix since it is composed of a vitreous/glassy phase. However, chamotte addition partially replaced quartz and feldspar in CHP-1, CHP-2, and CHP-3 samples, which almost approached the percentage of vitreous/glassy phase contained in the control samples (Dana et al., 2004). The above statement is supported by the commercial siliceous porcelain insulator phase composition: 5–25 wt.% of SiO_2 grains, 10–25 wt.% of $Al_6Si_2O_{13}$, and 65–80 wt.% of vitreous/glassy phase (Iqbal and Lee, 1999; Iqbal and Lee, 2000; Xie et al., 2012; Meng et al., 2014).

The relative intensity (RI) measurement for quantitative analysis was used to estimate the concentration of crystalline phases between

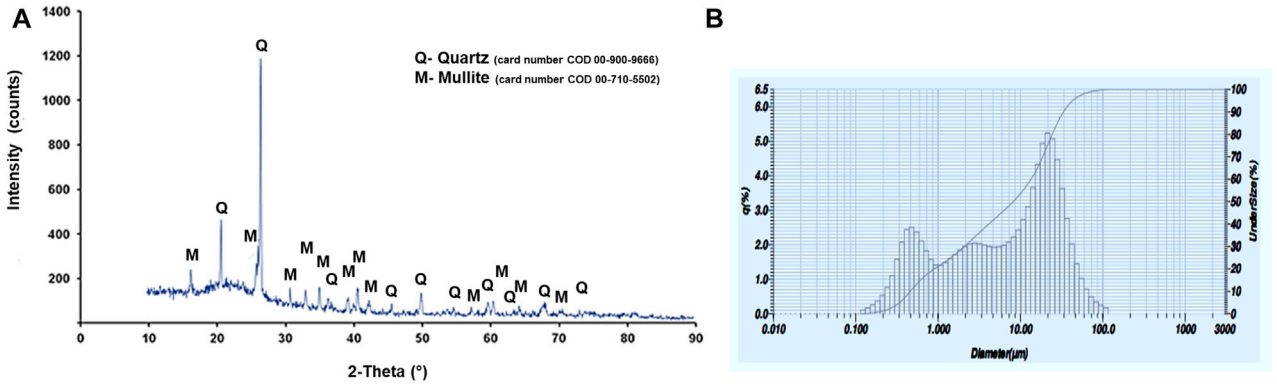

FIGURE 1
(A) XRD phase analysis of chamotte and **(B)** particle size distribution of chamotte.

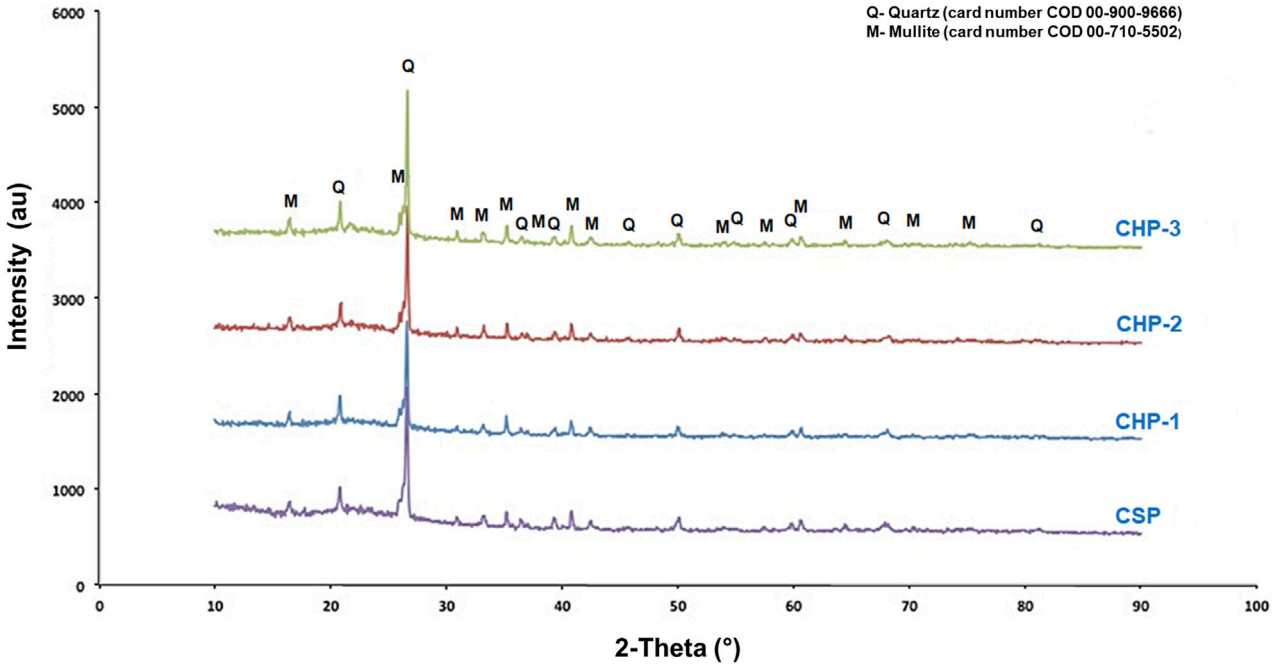

FIGURE 2
Comparative XRD phase analysis between the CSP formulation and siliceous porcelains with chamotte addition (CHP-1 to CHP-3).

CSP and CHP-3 compositions. According to the results, the CHP-3 formulation has a higher mullite concentration (59 wt.%) than the CSP formulation (56 wt.%). Meanwhile, the SiO_2 content in the CHP-3 formulation is 40 wt.% in contrast with the 43 wt.% in the CSP formulation.

A chemical analysis of each sintered formulation proposed in this study using the X-ray fluorescence method was carried out to corroborate and complement the XRD analysis. Table 1 shows the result of the XRF analysis. As observed, SiO_2 and Al_2O_3 are still the two principal oxides registered in the sintered formulations. Comparing the CSP formulation with the experimental sintered samples (with chamotte addition), SiO_2 concentration is not significantly affected. As chamotte was added, the SiO_2 content slightly decreased. However, there is an Al_2O_3 content increase as chamotte is added. Also, the content of TiO_2 and Fe_2O_3 impurities remains without significant changes. The Fe_2O_3 content in experimental samples does not affect the properties of the porcelain since it remains below 1 wt.% (Medeiros et al., 2019). The variation of Fe_2O_3 content is attributed to the iron content originating from chamotte as raw material, plus the concentration already present in the control porcelain formulation. The TiO_2 variation in concentration does not represent any problem that puts at risk the electro-technical porcelain properties.

On the other hand, there is an evident Na_2O content variation, as chamotte was added. This oxide concentration is affected mainly

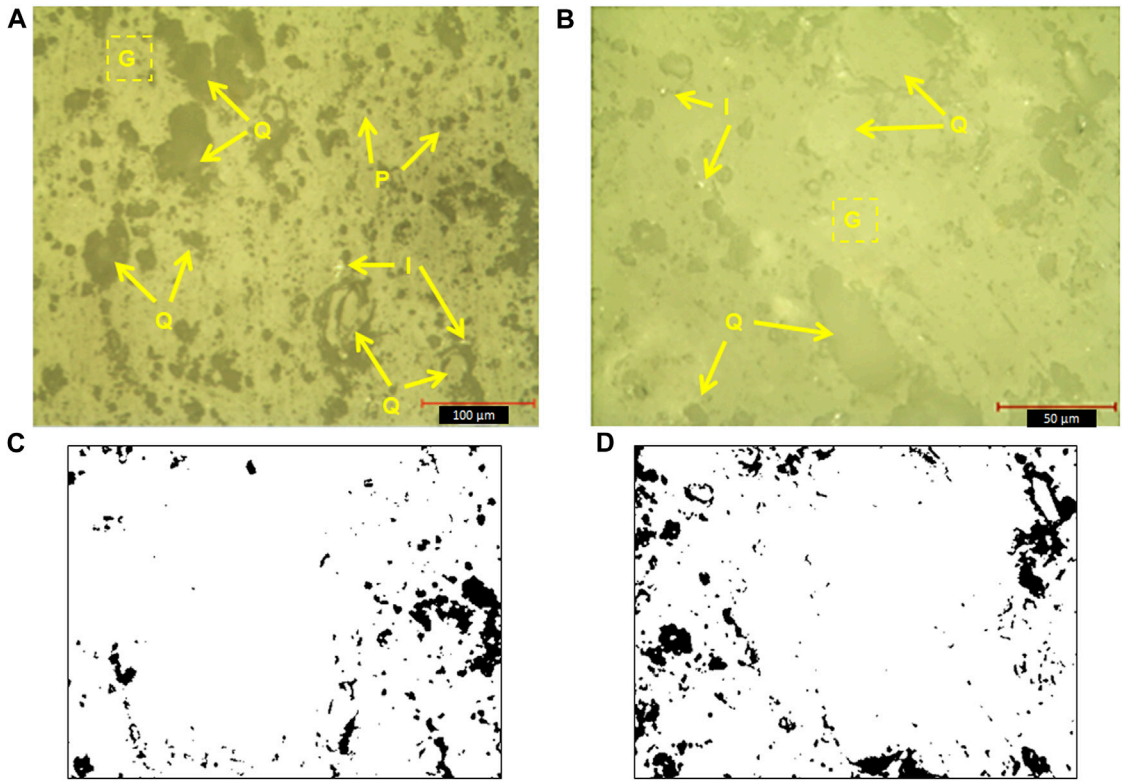

FIGURE 3
Microstructure of the control porcelain (CSP formulation) analyzed by optical microscopy. **(A)** 200X and **(B)** 400X (for more detail, see Rodriguez et al., 2019). **(C)** and **(D)** black and white images of CSP formulation showing porosity. Q = quartz, P = pores, G = vitreous matrix, I = impurities.

due to the chamotte addition since it contains a glassy phase rich in potassium and sodium. Na_2O concentration sharply increased from 2.334 wt.% (CSP formulation) to 8.02 wt.% (CHP-3 formulation). Meanwhile, K_2O negligibly decreased its concentration.

In summary, these chemical results support the XRD analysis, where the mullite phase increased as chamotte was added since the Al_2O_3 content increased in the chemical analysis. Also, the vitreous phase increase is observed with the Na_2O increase.

3.4 Microstructural analysis

Figures 3A, B shows the microstructural characteristics of the control formulation examined by the optical microscopy technique. An extended glassy/vitreous matrix with few SiO_2 particles enclosed in the matrix and impurities as little bright grains are noticed. Also, some pores well-dispersed in the matrix are observed (Figures 3C, D). The pore aspect in the CSP microstructure can be found as a quasi-spherical to an irregular morphology (with a size range between 10 and 20 µm). Also, it is possible to find some large and interconnected pores. The apparent porosity (open porosity) of the CSP sintered sample measured by the Archimedes proceeding was <0.01%. However, the closed and open pores are observed in the microstructure examination, which differed from the apparent porosity calculated.

Figure 4 shows the microstructure corresponding to the CHP-1 (Figures 4A–D), CHP-2 (Figures 4E–H), and CHP-3 (Figures 4I–L) experimental formulations analyzed by optical microscopy. The microstructure of CHP-1, CHP-2, and CHP-3 formulations is composed mainly of a glassy matrix, quartz grains, and impurities (bright particles). A peculiar aspect of these matrixes is that the chamotte addition increased the impurities number. A more homogeneous pore size (10–20 µm) and pore distribution are observed in the CHP-1, CHP-2, and CHP-3 experimental porcelain than in the control porcelain. This microstructural refinement might have originated from a higher glassy/vitreous phase percentage when the by-product material (porcelain chamotte) was added. At 1250°C, the glassy phase containing low melting point compounds and low viscosity around 1185°C to 1400°C (Conte et al., 2018) could penetrate, saturate, and make stable the pores in the porcelain material.

Figures 5A, B displays microscopy images in BSE mode (back-scattered electron mode), belonging to the CSP control formulation. A microstructure composed of an extended glassy matrix (light grey region) and SiO_2 particles (dark grey grains) enclosed in the matrix and rounded perimetral by peripheral microcracks is shown in Figures 5A, B. Also, well-distributed quasi-spherical pores in the microstructure are observed. The pore size varies from 10 to 20 µm. The total porosity (open and closed pores) is 9.24%, calculated by image analysis using ImageJ software. Some small bright grains as impurities are also identified in the microstructure. The cracks around the quartz grains originated from a critical β-α quartz phase change throughout the cooling stage, generating a bulk diminish (inner stress) of approximately 2%, as observed in

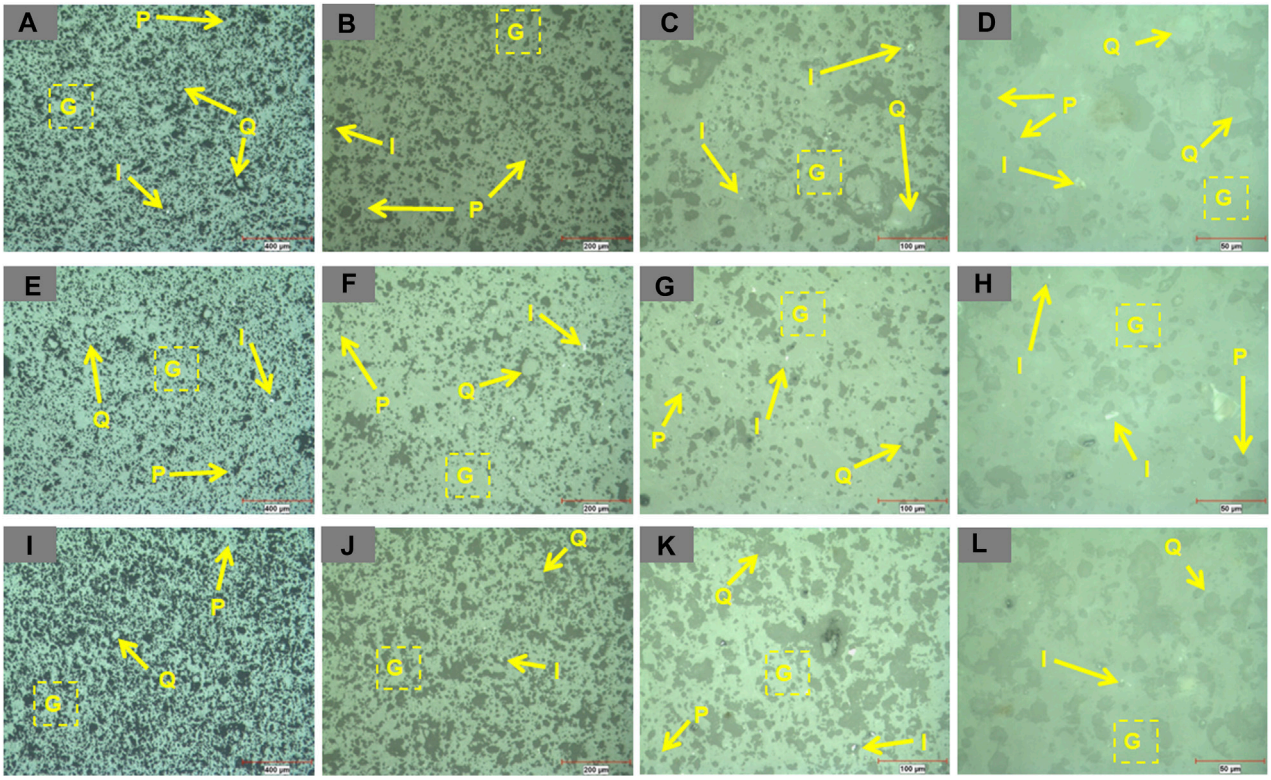

FIGURE 4
Microstructure analyzed by optical microscopy corresponding to the CHP-1 **(A–D)**, CHP-2 **(E–H)**, and CHP-3 **(I–L)** experimental formulations with chamotte addition (5, 10, and 15 wt.% respectively). Q = quartz, P = pores, G = vitreous matrix, I = impurities.

Figure 5B. As known, these circumferential cracks are beneficial to improve mechanical resistance when quartz particle size is smaller than 20 μm. Quartz particles larger than 30 μm develop detrimental circumferential cracks (Meng et al., 2012; Addis et al., 2023). The mean quartz particle is 11.53 μm, calculated by image analysis using ImageJ software.

Energy dispersive X-ray spectroscopy analysis (EDX) confirmed the presence of the following phases (see Figures 5C–E): i) a glassy matrix and ii) quartz particles. Bright particles with a sponge morphology corresponding to iron were observed. Also, brighter dense particles corresponding to titanium oxide particles were observed.

Figures 6 A–C shows the etched microstructure surface of the CSP control formulation. The etching process was carried out using 25% hydrofluoric acid. Relicted primary mullite (particle size < 0.5 μm in length) is detected in the vitreous matrix. Meanwhile, acicular mullite, known as secondary mullite, having a particle size from 3 to 5 μm (in length) with an interlocking arrangement, is also observed in the glassy phase. The interlocking organization of secondary mullite improves mechanical properties. The EDX results confirm both mullite-type phase presence (see Figures 6D, E).

Figures 7A–C shows BSE microscopy images of the CHP-1 to CHP-3 microstructure. Resembling microstructural features in the CHP-1 to CHP-3 samples were distinguished. The microstructure is made of a glassy matrix with some SiO_2 particles enclosed in it. The mean quartz particle sizes are 11.68 μm, 13.15 μm, and 15.08 μm, corresponding to CHP-1, CHP-2, and CHP-3, calculated by image analysis using ImageJ software. The pores are well-distributed in the microstructure. Most pores have a quasi-spherical morphology with a size from 10 to 20 μm. As known, spherical and homogeneous distributed pores benefit the mechanical strength of materials and contrast with abnormal-shaped pores that generate stress concentration that might act as a crack origin (Romero and Perez, 2015; Medeiros et al., 2019). Also, a closed and open porosity diminish is noticed as the chamotte was added (6.55%, 3.87%, and 4.12%, corresponding to CHP-1, CHP-2, and CHP-3, calculated by image analysis using ImageJ software). The porosity reduction might be connected to a more extended vitreous phase in the ceramic attributed to the chamotte addition (Stathis et al., 2004; Karamanov et al., 2006; Fernandes et al., 2020). This phenomenon can be attributed to a vitreous phase permeation as the temperature and sintering time increase, leading to porosity elimination via viscous-phase sintering. Also, it can be observed open porosity (large and interconnected pores) and groups of pores (clusters). Something remarkable is the apparent porosity of the ceramic samples since it is approximately 0.01%. At the highest chamotte additions, small bright particles (iron and titanium particles) were possibly detected by EDX analyses. Iron particles with a sponge morphology and bright titanium particles with a dense morphology are observed.

Secondary mullite particles with a size between 5 and 10 μm in the etched surface microstructure corresponding to CHP-1, CHP-2, and CHP-3 formulations are observed in Figures 8A–C. Secondary mullite forms during the chemical interaction between feldspar and

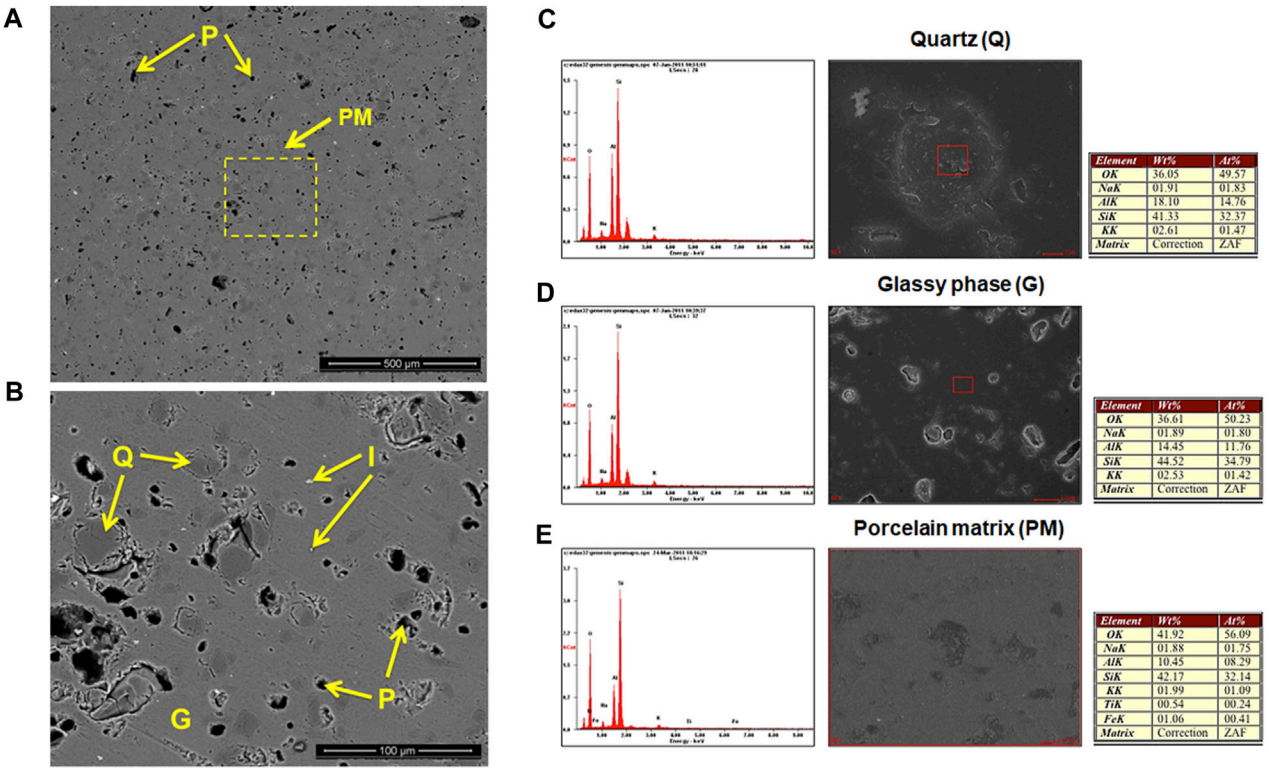

FIGURE 5
(A–B) Back-scattered electron microscopy (BSB) images corresponding to the CSP formulation. **(C)** quartz EDX, **(D)** glassy phase EDX, and **(E)** porcelain matrix EDX. Q = quartz, P = pores, G = vitreous/glassy matrix, I = impurities, and PM = porcelain matrix.

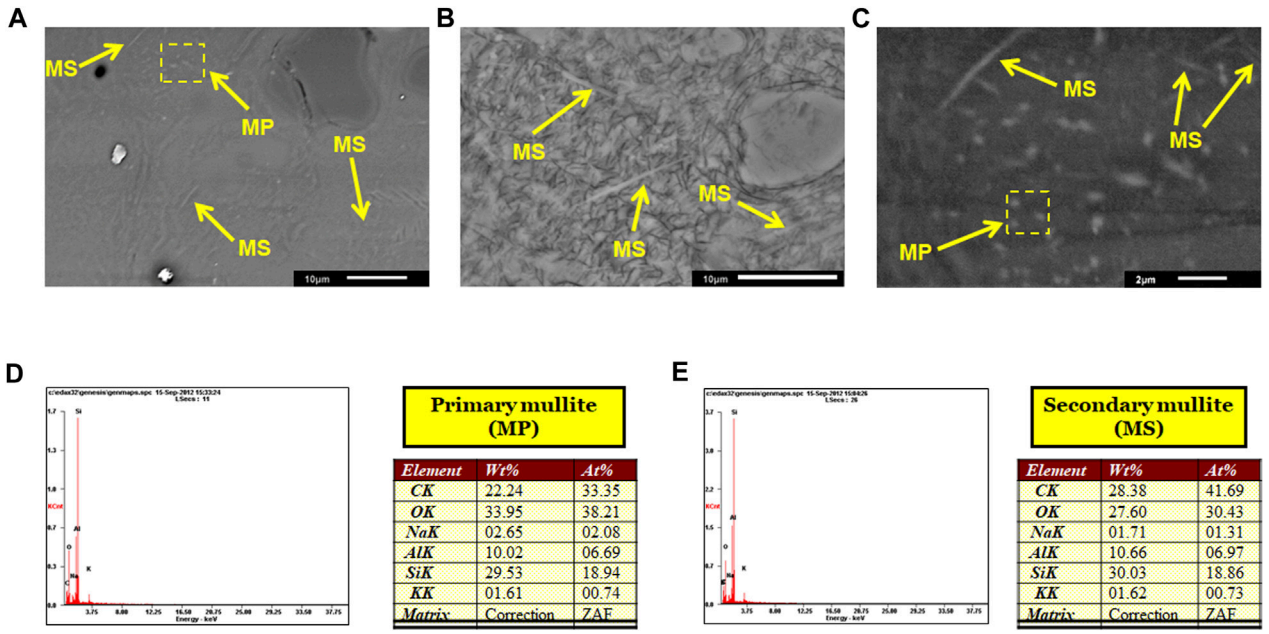

FIGURE 6
(A–C) Polished and etched microstructure (with 25% hydrofluoric acid) surface corresponding to the CSP formulation, **(D)** primary mullite EDX, and **(E)** secondary mullite EDX. MP = primary mullite and MS = secondary mullite.

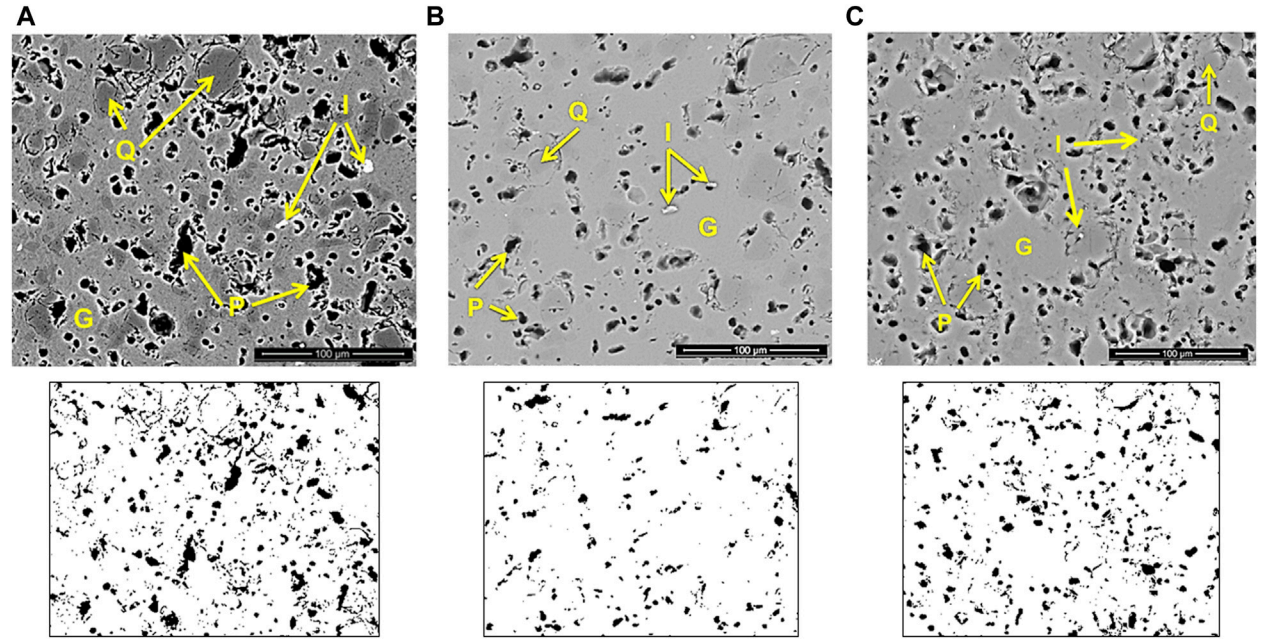

FIGURE 7
Sequence of back-scattered electron microscopy (BSB) images corresponding to the **(A)** CHP-1, **(B)** CHP-2, and **(C)** CHP-3 formulations. Q = quartz, P = pores, G = vitreous/glassy matrix, and I = impurities.

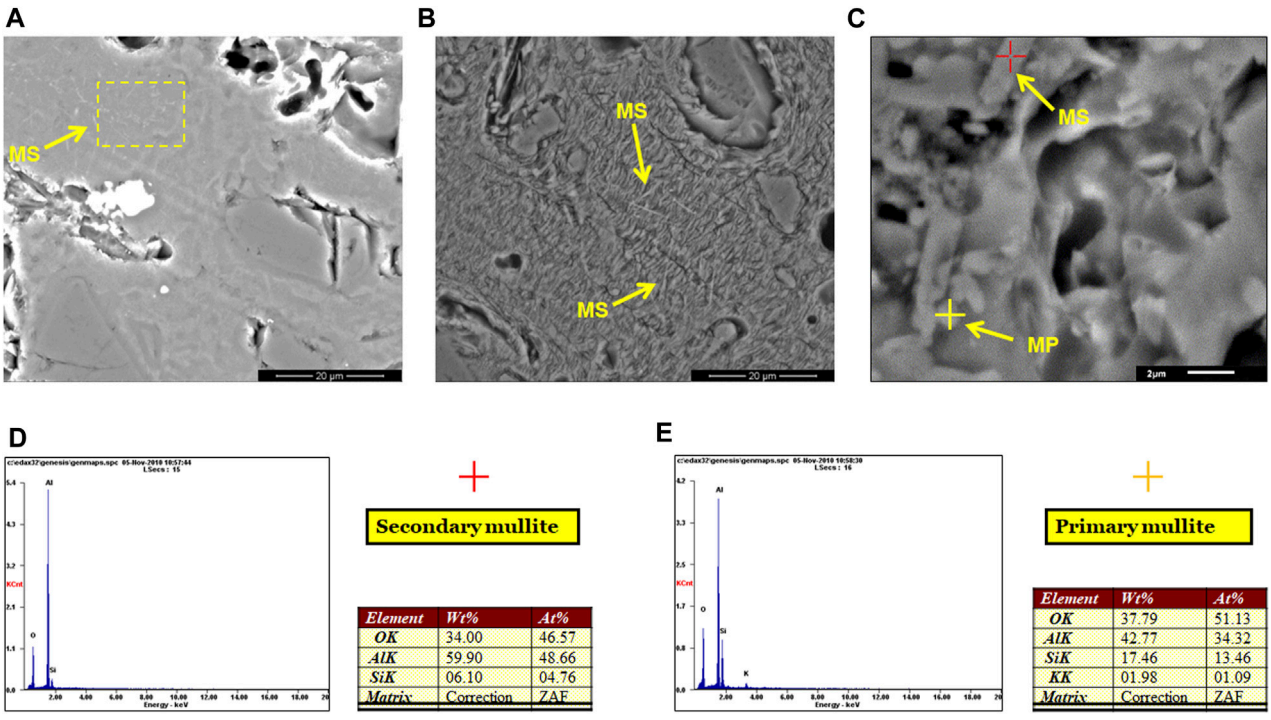

Element	Wt%	At%
OK	34.00	46.57
AlK	59.90	48.66
SiK	06.10	04.76
Matrix	Correction	ZAF

Element	Wt%	At%
OK	37.79	51.13
AlK	42.77	34.32
SiK	17.46	13.46
KK	01.98	01.09
Matrix	Correction	ZAF

FIGURE 8
SEM images and EDX microanalysis of the polished and etched microstructure surface corresponding to **(A)** CHP-3, **(B)** CHP-2, and **(C)** CHP-1 formulations. **(D)** Secondary mullite EDX and **(E)** primary mullite EDX. MP = primary mullite and MS = secondary mullite.

clay at circa 1200°C (Lee and Iqbal, 2001; Lee WE. et al., 2008; Montoya et al., 2010). Mullite gains crucial importance in porcelain bodies since mullite is a ceramic compound with well-recognized properties such as its high flexural strength of 100 MPa and high resemblance with the glassy-vitreous phase in terms of similar thermal expansion coefficients, $4.5 \times 10^{-6}°C^{-1}$and $3.0 \times 10^{-6}°C^{-1}$,

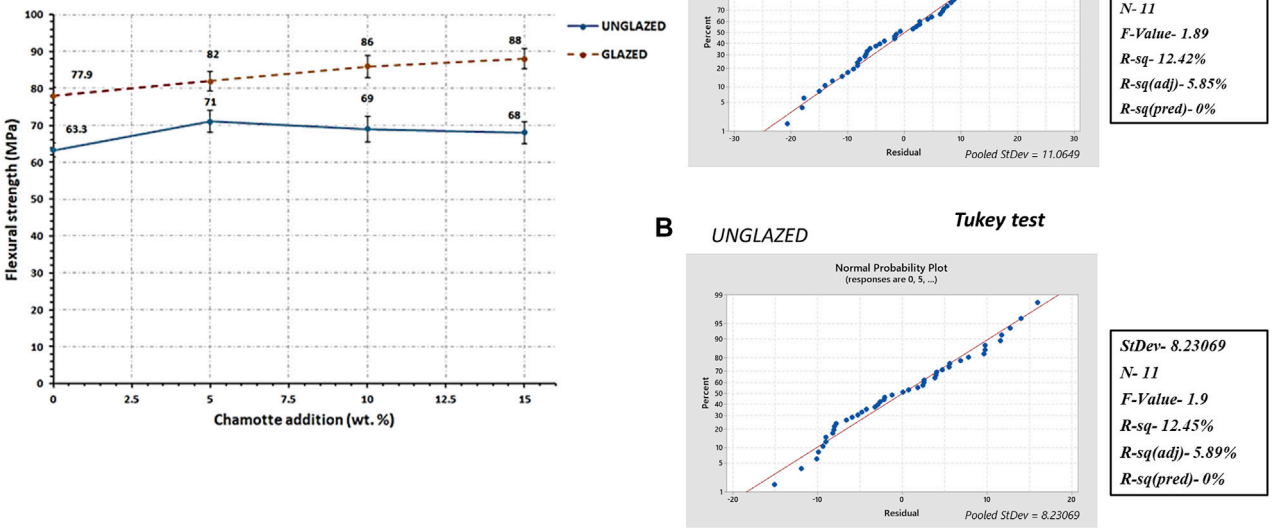

FIGURE 9
Effect of chamotte addition on the flexural strength resistance of unglazed and glazed siliceous porcelain. **(A)** Tukey test on glazed siliceous porcelain. **(B)** Tukey test on unglazed siliceous porcelain.

respectively (Liebermann, 2003; Meng et al., 2014; Figueirêdo et al., 2020). As mullite content increases in the porcelain microstructure, the mechanical behavior should be improved based on the strengthening concept related to mullite (Lee W. E. et al., 2008; Daniel et al., 2010). Sometimes, the mullite effect is not evident in mechanical strength, hardness, and elastic modulus enhancement since not depend only on mullite contents but the mullite morphology. Above 1250°C, mullite needles might grow in the axial and longitudinal axes, forming groups of needles (clusters) that restrict the properties improvement (Martín-Márquez et al., 2010; Mbakop et al., 2021). The EDX results confirm both mullite-type phase presence (see Figures 8D, E).

3.5 Mechanical behavior

Figure 9 displays the chamotte impact on the modulus of rupture of glazed and unglazed CSP formulation. The flexural strength of unglazed formulations increases when quartz and feldspar are substituted for chamotte. There was a maximum increase in resistance of 12.16% regarding CSP flexural strength (63.3 MPa). This improvement was accomplished by the CHP-1 formulation (71 MPa). After reaching this value, a slight decrement in mechanical resistance is observed. Therefore, the flexural strength dropped for CHP-2 (69 MPa) and CHP-3 (68 MPa) formulations considering the CHP-1 flexural strength. However, the improvement in flexural strength for CHP-2 and CHP-3 formulations was 9% and 7.42%, respectively, about the CSP strength value. On the other hand, flexural strength values lower than those obtained in chamotte-containing porcelain samples were reported in the production of porcelain electrical insulators replacing feldspar with Sugarcane bagasse ash under similar conditions (SCBA-10 wt.%, sintering temperature-1250°C, and FS-42.5 MPa) (Addis et al., 2023).

This unexpected mechanical behavior might be attributed to the glassy phase increase in the body due to the substitution of quartz and feldspar for chamotte. As known, the strength in clay-quartz-feldspar porcelains is controlled by the crystalline phase appearance frequency (Buchanan, 1991). Therefore, a vitreous-glassy phase increase could represent a drop in the mechanical characteristics (Amigó et al., 2004; Romero and Pérez, 2015). Stathis et al. and Karamanov et al. reported that the quartz replacement mainly increments the sodium and potash oxides, decreasing the strength (Stathis et al., 2004; Karamanov et al., 2006).

Additionally, it must be contemplated that a higher mullite content in the porcelain body originating from the chamotte demands a higher sintering temperature to develop improved mechanical properties. It is worth mentioning that mullite formation begins from ~1050°C to 1200°C, completing their transformation at 1200°C to 1400°C under standard sintering parameters (Güngör and Ay, 2018).

Meanwhile, glaze porcelain samples develop higher flexural strength than unglazed samples. The resistance in glazed bodies increases as the chamotte was added to the control formulation. Higher flexural strengths were obtained (concerning the value of CSP formulation) for CHP-1, CHP-2, and CHP-3 formulations, which are 5.26%, 10.39%, and 12.96%, respectively. The maximum flexural strength was reached by CHP-3 formulation (88 MPa). As known, the areas nearest to the external face faced more critical stress than other areas under pressure. Therefore, large pores close to the surface area are more prompting to originate fracture. There are

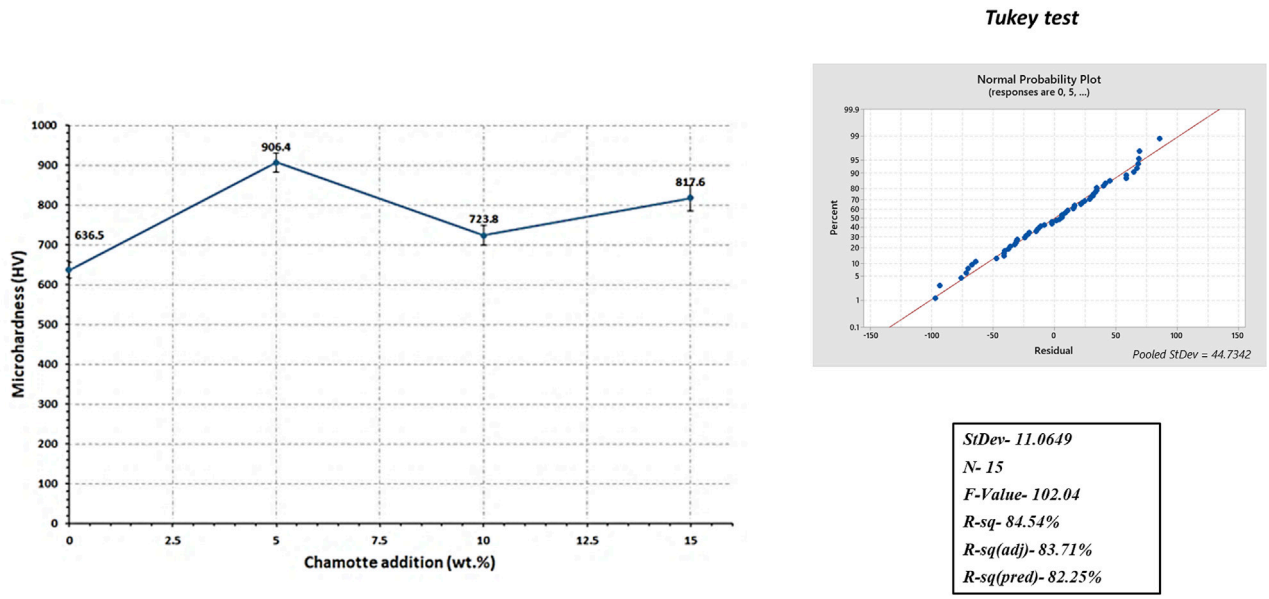

FIGURE 10
Effect of chamotte addition on the HV microhardness of siliceous porcelain. Tukey test on the HV microhardness of siliceous porcelain.

TABLE 2 Economic benefit of chamotte reuse.

Volume of electrical insulator production 2022 (12,562 tons)			
Concepts	Cost per ton (USD)	Material consumption (tons)	Total cost (USD)
Quartz	180	248	44,640
Sodium feldspar	220	248.62	54,696.4
Chamotte production expenses	78	497.4	38,797.2
Chamotte treatment/disposal expenses	15	497.4	7,461
Annual benefits	68,000.2 (USD)		

two well-documented mechanisms to improve the flexural strength of the porcelain body. i) The glaze can permeate the pores on the superficial area and form a smoother external face that reduces fissures and slows down cracking. ii) The glaze develops a coating with a distinct chemical constitution that modifies the stress effect in the body (Haberko and Haberko, 1975; Xie et al., 2012). These two mechanisms improve the flexural resistance of the experimental porcelain bodies.

According to the IEC60672-3 standard, the three experimental compositions achieved superior strength than the normalized values (unglazed-50 MPa and glazed-60 MPa) for siliceous porcelain bodies. These experimental formulations are mechanically attractive for electro-technical operations as insulators, being an innovative and ecological alternative.

Figure 10 shows the results of the HV microhardness test carried out in the experimental formulations. As observed, considering the value achieved by the CSP formulation, the three experimental formulations surpass the CSP value (636.5 HV). The CHP-1 formulation achieved the highest microhardness value (906.4 HV). That means an enhancement of 42% compared to the CSP formulation. However, a hardness decrease based on the CHP-1 formulation is observed for the CHP-2 formulation (723.8 HV). Despite this decrease in hardness, the hardness is still higher than the CSP formulation. The CHP-3 formulation reached an HV hardness of 817.6.

Although a non-linear tendency is observed, the improved hardness performance can be connected with a superior mullite presence in the porcelain body, in agreement with the X-ray diffraction analysis (Al-Hilli and Al-Rasoul, 2013; Harabi et al., 2017; Belhouchet et al., 2019). The diminished HV hardness at higher chamotte addition might be attributed to a more extended vitreous phase in the bodies.

3.6 Thermal behavior

The linear expansion coefficients calculated for CSP, CHP-1, CHP-2, and CHP-3 formulations (100°C to 1200°C) were $7.63 \times 10^{-6}°C^{-1}$, $7.6 \times 10^{-6}°C^{-1}$, $7.5 \times 10^{-6}°C^{-1}$, and $7.17 \times 10^{-6}°C^{-1}$, respectively. As observed, there is a decrease in the linear thermal expansion coefficient

as the chamotte addition increases in the body. This response might be related to a lower SiO_2 concentration in the body. Typically, a higher thermal expansion is anticipated at higher SiO_2 concentrations. This behavior is attributed to the SiO_2 polymorphism, contributing to a more extended crack formation. Meanwhile, more thermal stability than SiO_2 is observed when a more extended mullite content is found due to chamotte addition (Ghaffari et al., 2014; Gungor and Ay, 2018).

3.7 Environmental and economic impact of chamotte reuse

It is estimated that the annually wasted electrical porcelain insulators in some Latin-American countries can be c.a. 25,000 tons (Campos and Paulon, 2015). These insulators are often discarded, deteriorating the environment. Table 2 shows an annual cost analysis benefit of a local Mexican electrical porcelain insulators company using chamotte as raw material for electrical porcelain insulators manufacture. The analysis is based on a volume of electrical porcelain insulator production of 12,562 tons/annual and 15 wt.% of quartz-feldspar replacement by chamotte. The benefits are 68,000.2 (USD) annually. Meanwhile, replacing quartz for chamotte at 15 wt.%, the save is 57,943.8 (USD). The binary replacement has an improvement of 14.78% against the monomodal alternative (quartz for chamotte).

Taking into account the above benefits, the partial replacement of traditional raw materials by industrial waste in the manufacture of conventional electrical porcelain insulators is a "green" practice that represents environmental and economic benefits such as: i) efficient management for the chamotte, ii) reducing the consumption of the non-renewable and overexploited quartz and feldspar sources, iii) the use of an alternative raw material with a lower price (i.e., 73 $/ton) compared to quartz (i.e., 180 $/ton) and feldspar (i.e., 220 $/ton), and iv) saving the extensive energy consumption during sintering since chamotte contains as a final phase, the mullite in a sintered porcelain insulator.

4 Conclusion

The study of the effect of binary raw materials replacement (quartz and feldspar) by porcelain chamotte on the properties of electro-technical porcelain was carried out in this research. The chamotte waste fit the circular economy concept since it accomplished the new industrial model focused on resource optimization (saving high-grade feldspar minerals and good quality quartz) and waste reduction.

Our work contributed to the following finding:

There is a proportional increase in density as chamotte was added to the experimental porcelain due to a higher mullite proportion. The water absorption and apparent porosity reached a value <0.01%, representing a desirable property of electro-technical siliceous porcelains.

The modulus of rupture of glazed and unglazed experimental samples is superior to the technical data specified by the IEC standard (60 MPa and 50 MPa, respectively). The modulus of rupture in unglazed samples was enhanced by ~12% by substituting 5 wt.% of feldspar and quartz with by-product material (porcelain chamotte) in the CSP control composition. Meanwhile, the modulus of rupture in glazed samples was enhanced by ~12.96% by replacing 15 wt.% of feldspar and quartz with porcelain chamotte in the CSP control composition. This percentage replacement represents an invaluable resource optimization, saving high-grade feldspar minerals and good-quality quartz consumption.

Microhardness shows an incremental tendency as chamotte is increased in the ceramic body. This response might be related to a superior mullite presence in the ceramic body. A higher mullite concentration was corroborated by the XRD and SEM analysis.

The linear thermal expansion coefficients suffer a decrement as the chamotte increases in the body. This tendency might originate from the quartz reduction since it prevents quartz polymorphism as the temperature rises. Meanwhile, a chamotte increment led to a higher mullite presence in the body, resulting in higher thermal stability than quartz.

According to the final properties observed, the possibility of using by-product material (porcelain chamotte) in a siliceous porcelain composition has been favorable with remarkable properties. In the present research work, an innovative ceramic product that fits the circular economy concept was produced as an interesting possible choice for electro-technical functions.

Data availability statement

The original contributions presented in the study are included in the article/Supplementary Material, further inquiries can be directed to the corresponding author.

Author contributions

ER: Conceptualization, Data curation, Formal Analysis, Supervision, Writing–original draft, Writing–review and editing, Investigation. LD-T: Formal Analysis, Methodology, Writing–review and editing. YG-C: Formal Analysis, Methodology, Writing–review and editing. JL-P: Formal Analysis, Investigation, Methodology, Writing–review and editing.

Funding

The authors declare that no financial support was received for the research, authorship, and/or publication of this article.

Conflict of interest

The authors declare that the research was conducted in the absence of any commercial or financial relationships that could be construed as a potential conflict of interest.

Publisher's note

All claims expressed in this article are solely those of the authors and do not necessarily represent those of

their affiliated organizations, or those of the publisher, the editors and the reviewers. Any product that may be evaluated in this article, or claim that may be made by its manufacturer, is not guaranteed or endorsed by the publisher.

Supplementary material

The Supplementary Material for this article can be found online at: https://www.frontiersin.org/articles/10.3389/fmats.2023.1322898/full#supplementary-material

References

Addis, T., Wondemagegnehu, E. B., Zereffa, E. A., Tullu, A. M., and Brehane, B. (2023). Sugarcane Bagasse ash substituent feldspar for the production of porcelain electrical insulators. *Ceram. Int.* 49, 7727–7736. doi:10.1016/j.ceramint.2022.10.279

Ahmed Salem, A., Kwan, Y., Abdul-Malek, Z., Al-Gailani, S. A., and Tan, C. W. (2022). Flashover voltage of porcelain insulator under various pollution distributions: experiment and modeling. *Electr. Power Syst. Res.* 208, 107867. doi:10.1016/j.epsr.2022.107867

Al-Gheilani, A., Rowe, W., Li, Y., and Wong, K. L. (2017). Stress control methods on a high voltage insulator: a review voltage insulator: a review. *Energy Procedia* 110, 95–100. doi:10.1016/j.egypro.2017.03.112

Al-Hilli, M. F., and Al-Rasoul, K. T. (2013). Characterization of alumino-silicate glass/kaolinite composite. *Ceram. Int.* 39, 5855–5862. doi:10.1016/j.ceramint.2012.12.102

Alhumoud, J. M. (2005). Municipal solid waste recycling in the Gulf co-operation council states. *Resour. Conserv. Recycl.* 45, 142–158. doi:10.1016/j.resconrec.2005.01.010

Almeida, E. P., Carreiro, M. E. A., Rodrigues, A. M., Ferreira, H. S., Santana, L. N. L., Menezes, R. R., et al. (2021). A new eco-friendly mass formulation based on industrial mining residues for the manufacture of ceramic tiles. *Ceram. Int.* 47, 11340–11348. doi:10.1016/j.ceramint.2020.12.260

Almeida, M., Simões, F., Días, F., and Amado, A. (2016). Ceramic industry contribution to a circular economy. *Present. A. T. Congr. Inovation Sustain. Constr. CINCOS*.

Altimari, F., Andreola, F., Benassi, P. P., Lancellotti, I., and Barbieri, L. (2023). Pumice and lapillus scraps: new national environmental-friendly chance for the production of ceramic tiles. *Ceram. Int.* 49, 38743–38753. doi:10.1016/j.ceramint.2023.09.211

Amigó, J. M., Clausell, J. V., Esteve, V., Delgado, J. M., Reventós, M. M., Ochando, L. E., et al. (2004). X-ray powder diffraction phase analysis and thermomechanical properties of silica and alumina porcelains. *J. Eur. Ceram. Soc.* 24, 75–81. doi:10.1016/S0955-2219(03)00119-5

Amigó, J. M., Serrano, F. J., Kojdecki, M. A., Bastida, J., Esteve, V., Reventós, M. M., et al. (2005). X-ray diffraction microstructure analysis of mullite, quartz and corundum in porcelain insulators. *J. Eur. Ceram. Soc.* 25, 1479–1486. doi:10.1016/j.jeurceramsoc.2004.05.019

Awoyera, P. O., Ndambuki, J. M., Akinmusuru, J. O., and Omole, D. O. (2016). Characterization of ceramic waste aggregate concrete. *HBRC J.* 14, 282–287. doi:10.1016/j.hbrcj.2016.11.003

Belhouchet, K., Bayadi, A., Belhouchet, H., and Romero, M. (2019). Improvement of mechanical and dielectric properties of porcelain insulators using economic raw materials. *Bol. Soc. Esp. Ceram. Vidr.* 58, 28–37. doi:10.1016/j.bsecv.2018.05.004

Benavidez, E., Caligaris, M., Quaranta, N., and Boccaccini, A. (1999). "Electric companies wastes as ceramic raw material," in Sixth Conference and Exhibition of the European Ceramic Society, Brighton, England, July, 1999.

Bragança, S. R., and Bergman, C. P. (2004). Microestrutura e propriedades de porcelanas. *Cerámica* 50, 291–299. doi:10.1590/s0366-69132004000400003

Brito, J., and Saikia, N. (2013). *Recycled aggregate in concrete. Green energy and technology*. Berlin, Germany: Springer London Ltd, 23–80.

Buchanan, R. C. (1991). *Properties of ceramic insulators. Ceramic materials for electronic*. New York, NY, USA: Marcel Dekker Inc.

Caligaris, R., Quaranta, N., Caligaris, M., and Benavidez, E. (2000). Materias primas no tradicionales en la industria cerámica. *Bol. Soc. Esp. Ceram. V.* 39 (5), 623–626. doi:10.3989/cyv.2000.v39.i5.779

Campos, M. A., and Paulon, V. A. (2015). Utilização de agregados alternativos de isoladores elétricos de porcelana em concretos. concreto y cemento. *Investig. Desarro.* 7, 30–43.

Cicek, B., Karadagli, E., and Duman, F. (2018). Valorisation of boron mining wastes in the production of wall and floor tiles. *Constr. Build. Mater.* 179, 232–244. doi:10.1016/j.conbuildmat.2018.05.182

Conte, S., Zanelli, C., Ardit, M., Cruciani, G., and Dondi, M. (2018). Predicting viscosity and surface tension at high temperature of porcelain stoneware bodies: a methodological approach methodological approach. *Materials.* 11, 1–16. doi:10.3390/ma11122475

Conte, S., Zanelli, C., Molinari, C., Guarini, G., and Dondi, M. (2020). Glassy wastes as feldspar substitutes in porcelain stoneware tiles: thermal behaviour and effect on sintering process. *Mater. Chem. Phys.* 256, 123613. doi:10.1016/j.matchemphys.2020.123613

Contreras, J. E., and Rodríguez, E. A. (2017). Nanostructured insulators – a review of nanotechnology concepts for outdoor ceramic insulators. *Ceram. Int.* 43, 8545–8550. doi:10.1016/j.ceramint.2017.04.105

Cregut, M., Bedas, M., Durand, M.-J., and Thouand, G. (2013). New insights into polyurethane biodegradation and realistic prospects for the development of a sustainable waste recycling process. *Biotechnol. Adv.* 31, 1634–1647. doi:10.1016/j.biotechadv.2013.08.011

Dana, K., Das, S., and Das, K. S. (2004). Effect of substitution of fly ash for quartz in triaxial Kaolin-Quartz-Feldspar system. *J. Eur. Ceram. Soc.* 24, 3169–3175. doi:10.1016/j.jeurceramsoc.2003.10.008

Deniel, S., Tessier-Doyen, N., Dublanche-Tixier, C., Chateigner, D., and Blanchart, P. (2010). Processing and characterization of textured mullite ceramics from phyllosilicates. *J. Eur. Ceram. Soc.* 12, 2427–2434. doi:10.1016/j.jeurceramsoc.2010.04.029

Fassbinder, G. (2002). *A new ceramic body concept for high strength HV insulators*. Stuttgart, Germany: LAPP.

Fernandes, J. V., Guedes, D. G., Da Costa, F. P., Rodrigues, A. M., Neves, G. D. A., Menezes, R. R., et al. (2020). Sustainable ceramic materials manufactured from ceramic formulations containing quartzite and scheelite tailings. *Sustainability* 12, 9417. doi:10.3390/su12229417

Figueirêdo, J. M. R. D., Costa, F. P. D., Fernandes, J. V., Rodrigues, A. M., Neves, G. D. A., Menezes, R. R., et al. (2020). Development of scheelite tailings-based ceramic formulations with the potential to manufacture porcelain tiles, semi-stoneware and stoneware. *Materials* 13, 5122. doi:10.3390/ma13225122

Garcia-Muiña, F., González-Sánchez, R., Ferrari, A., and Settembre-Blundo, D. (2018). The paradigms of industry 4.0 and circular economy as enabling drivers for the competitiveness of businesses and territories: the case of an Italian ceramic tiles manufacturing company. *Soc. Sci.* 7, 255. doi:10.3390/socsci7120255

Geissdoerfer, M., Savaget, P., Bocken, N. M. P., and Hultink, E. J. (2017). The Circular Economy – a new sustainability paradigm? *J. Clean. Prod.* 143, 757–768. doi:10.1016/j.jclepro.2016.12.048

Ghaffari, M., Salahi, E., and Rajabi, A. (2014). Effect of alumina substitution on porosity and thermal expansion of triaxial porcelain-like bodies. *J. Ceram. Sci. Technol.* 5, 287–292. doi:10.4416/JCST2014-00021

Gharibi, H., Mostofinejad, D., Bahmani, H., and Hadadzadeh, H. (2022). Improving thermal and mechanical properties of concrete by using ceramic electrical insulator waste as aggregates. *Constr. Build. Mater.* 338, 127647. doi:10.1016/j.conbuildmat.2022.127647

Gress, R. I., and Leshehenko, N. P. (1967). *Increasing the porcelain pitcher content in high voltage porcelain bodies*. Berlin, Germany: Springer.

Gubanski, S. (2010). Outdoor high voltage insulation [Editorial. *Trans. Dielectr. Electr. Insulation* 17, 325. doi:10.1109/tdei.2010.5448084

Güngör, F., and Ay, N. (2018). The effect of particle size of body components on the processing parameters of semi transparent porcelain. *Ceram. Int.* 44, 10611–10620. doi:10.1016/j.ceramint.2018.03.086

Haberko, M., and Haberko, K. (1975). Effect of glaze on strength of high tension porcelain. *Ceramurg. Int.* 1, 28–32. doi:10.1016/0390-5519(75)90036-8

Harabi, A., Kasrani, S., Foughali, L., Serradj, I., Benhassine, M. T., and Kitouni, S. (2017). Effect of TiO_2 additions on densification and mechanical properties of new mulltifunction resistant porcelains using economic raw materials. *Ceram. Int.* 43, 5547–5556. doi:10.1016/j.ceramint.2017.01.081

Harper, C. (2001). *Handbook of ceramics, glasses, and diamonds*. Australia: McGrawHill Professional.

Iqbal, Y., and Lee, W. (1999). Fired porcelain microstructures revisited. *J. Am. Ceram. Soc.* 82, 3584–3590. doi:10.1111/j.1151-2916.1999.tb02282.x

Iqbal, Y., and Lee, W. (2000). Microstructural evolution in triaxial porcelain. *J. Am. Ceram. Soc.* 83, 3121–3127. doi:10.1111/j.1151-2916.2000.tb01692.x

Karamanov, A., Karamanova, E., Ferrari, A. M., Ferrante, F., and Pelino, M. (2006). The effect of fired scrap addition on the sintering behaviour of hard porcelain. *Ceram. Int.* 32, 727–732. doi:10.1016/j.ceramint.2005.05.009

Kelestemur, O., Yildiz, S., Gökçer, B., and Arici, E. (2014). Statistical analysis for freeze thaw resistance of cement mortars containing marble dust and glass fiber. *Mater Des.* 60, 548–555. doi:10.1016/j.matdes.2014.04.013

Khan, M. S., Sohail, M., Khattak, N. S., and Sayed, M. (2016). Industrial ceramic waste in Pakistan, valuable material for possible applications. *J. Clean. Prod.* 139, 1520–1528. doi:10.1016/j.jclepro.2016.08.131

Lassinantti Gualtieri, M., Mugoni, C., Guandalini, S., Cattini, A., Mazzini, D., Alboni, C., et al. (2018). Glass recycling in the production of low-temperature stoneware tiles. *J. Clean. Prod.* 197, 1531–1539. doi:10.1016/j.jclepro.2018.06.264

Lee, W. E., and Iqbal, Y. (2001). Influence of mixing on mullite formation in porcelain. *J. Eur. Ceram. Soc.* 14, 2583–2586. doi:10.1016/S0955-2219(01)00274-6

Lee, W. E., Jayaseelan, D. D., and Zhang, S. (2008b). Solid-liquid interactions: the key to microstructural evolution in ceramics. *J. Eur. Ceram. Soc.* 7, 1517–1525. doi:10.1016/j.jeurceramsoc.2007.12.010

Lee, W. E., Souza, G. P., McConville, C. J., Tarvornpanich, T., and Iqbal, Y. (2008a). Mullite formation in clays and clay-derived vitreous ceramics. *J. Eur. Ceram. Soc.* 2, 465–471. doi:10.1016/j.jeurceramsoc.2007.03.009

Liebermann, J. (2000). Reliability of materials for high-voltage insulators. *Am. Ceram. Soc. Bull.* 79, 55–58.

Liebermann, J. (2003). Microstructure properties and product quality of strength-stressed high-voltage insulators. *Am. Ceram. Soc. Bull.* 2, 39–46B.

Liebermann, J. (2012). High-voltage insulators: basics and trends for producers, users and students. in *Fraunhofer Institute for Ceramic Technologies and Systems IKTS*. Schulze.

Liu, T., Zhang, J., Wu, J., Liu, J., Li, C., Ning, T., et al. (2019). The utilization of electrical insulators waste and red mud for fabrication of partially vitrified ceramic materials with high porosity and high strength. *J. Clean. Prod.* 223, 790–800. doi:10.1016/j.jclepro.2019.03.162

Locks, M., Arcaro, S., Bergmann, C. P., Ribeiro, M. J., Raupp-Pereira, F., and Montedo, O. R. K. (2021). Effect of feldspar substitution by basalt on pyroplastic behaviour of porcelain tile composition. *Materials* 14, 3990. doi:10.3390/ma14143990

Martín-Márquez, J., Rincón, J. M., and Romero, M. (2010). Effect of microstructure on mechanical properties of porcelain stoneware. *J. Eur. Ceram. Soc.* 30, 3063–3069. doi:10.1016/j.jeurceramsoc.2010.07.015

Marvila, M. T., De Azevedo, A. R. G., Alexandre, J., Colorado, H., Pereira Antunes, M. L., and Vieira, C. M. F. (2021). Circular economy in cementitious ceramics: replacement of hydrated lime with a stoichiometric balanced combination of clay and marble waste. *Int. J. Appl. Ceram. Tech.* 18, 192–202. doi:10.1111/ijac.13634

Mbakop, T. T., Deutou, J. G. N., Boubakar, L., Billong, N., Melo, U. C., Kamseu, E., et al. (2021). Enhancing the crystallization phenomena and strength of porcelain stoneware: the role of CaO. *J. Therm. Anal. Calorim.* 144, 91–106. doi:10.1007/s10973-020-09323-5

Medeiros, P. S. S. D., Lira, H. D. L., Rodriguez, M. A., Menezes, R. R., Neves, G. D. A., and Santana, L. N. D. L. (2019). Incorporation of quartzite waste in mixtures used to prepare sanitary ware. *J. Mater. Res. Technol.* 8, 2148–2156. doi:10.1016/j.jmrt.2019.02.001

Mehta, N. S., Sahu, P. K., Tripathi, P., Pyare, R., and Majhi, M. R. (2018). Influence of alumina and silica addition on the physico-mechanical and dielectric behavior of ceramic porcelain insulator at high sintering temperature. *Bol. Soc. Esp. Ceram. Vidr.* 57, 151–159. doi:10.1016/j.bsecv.2017.11.002

Meng, Y., Gong, G., Wei, D., and Xie, Y. (2016). *In situ* high temperature X-ray diffraction study on high strength aluminous porcelain insulator with the Al2O3-SiO2-K2O-Na2O system. *Appl. Clay Sci.* 132–133, 760–767. doi:10.1016/j.clay.2016.07.014

Meng, Y., Gong, G., Wei, D., Xie, Y., and Yin, Z. (2014). Comparative microstructure study of high strength alumina and bauxite insulator. *Ceram. Int.* 40, 10677–10684. doi:10.1016/j.ceramint.2014.03.052

Meng, Y., Gong, G., Wu, Z., Yin, Z., Xie, Y., and Liu, S. (2012). Fabrication and microstructure investigation of ultra-high-strength porcelain insulator. *J. Eur. Ceram. Soc.* 32, 3043–3049. doi:10.1016/j.jeurceramsoc.2012.04.015

Merga, A., Murthy, H. C. A., Amare, E., Ahmed, K., and Bekele, E. (2019). Fabrication of electrical porcelain insulator from ceramic raw materials of Oromia region, Ethiopia. *Heliyon* 5, e02327. doi:10.1016/j.heliyon.2019.e02327

Mohamed, K. R., Mousa, S. M., and El-Bassyouni, G. T. (2014). Fabrication of nano structural biphasic materials from phosphogypsum waste and their *in vitro* applications. *Mater. Res. Bull.* 50, 432–439. doi:10.1016/j.materresbull.2013.11.023

Mohammad, S. K., Mohammad, S., Noor, S. K., and Murtaza, S. (2016). Industrial ceramic waste in Pakistan, valuable material for possible applications. *J. Clean. Prod.* 139, 1520–1528. doi:10.1016/j.jclepro.2016.08.131

Montoya, N., Serrano, F. J., Reventós, M. M., Amigo, J. M., and Alarcón, J. (2010). Effect of TiO2 on the mullite formation and mechanical properties of alumina porcelain. *J. Eur. Ceram. Soc.* 4, 839–846. doi:10.1016/j.jeurceramsoc.2009.10.009

Naenudon, S., Wongsa, A., Ekprasert, J., Sata, V., and Chindaprasirt, P. (2023). Enhancing the properties of fly ash-based geopolymer concrete using recycled aggregate from waste ceramic electrical insulator. *J. Build. Eng.* 68, 106132. doi:10.1016/j.jobe.2023.106132

Nodeh, A. A. (2017). Influence of bone porcelain scraps on the physical characteristics and phase composition of a hard porcelain body. *Bol. Soc. Esp. Ceram. Vidr.* 56, 113–118. doi:10.1016/j.bsecv.2017.04.003

Ogbonda, C., and Onuchuku, P. (2021). Enhancement of mechanical and dielectric properties of porcelain insulators using locally available raw materials. *Afr. J. Innovations Pure Appl. Sci.* 11.

Owoeye, S. S., Toludare, T. S., Isinkaye, O. E., and Kingsley, U. (2019). Influence of waste glasses on the physico-mechanical behavior of porcelain ceramics. *Bol. Soc. Esp. Ceram. Vidr.* 58, 77–84. doi:10.1016/j.bsecv.2018.07.002

Penteado, C. S. G., Viviani De Carvalho, E., and Lintz, R. C. C. (2016). Reusing ceramic tile polishing waste in paving block manufacturing. *J. Clean. Prod.* 112, 514–520. doi:10.1016/j.jclepro.2015.06.142

Pereira, V., Geraldo, R., Baldusco, R., and Camarini, G. (2022). Porcelain waste from electrical insulators in self-leveling mortar: materials characterization and properties. *J. Build. Eng.* 61, 105297. doi:10.1016/j.jobe.2022.105297

Piva, D. H., Piva, R. H., Venturini, J., Ramon, J., Caldas, V., Morelli, M. R., et al. (2016). Effect of Fe_2O_3 content on the electrical resistivity of aluminous porcelain applied to electrical insulators. *Ceram. Int.* 42, 5045–5052. doi:10.1016/j.ceramint.2015.12.016

Quaranta, N., Caligaris, M., and Benavidez, E., 1998. Recycling electric insulators as a way to have mullite, 3 International Meeting of Pacific Rim Ceramic Societies, PacRim. Kyongju, Corea, September, 1998.

Ren, Z. F., Xiao, X., Chen, D. Y., Bi, X. H., Huang, B., Liu, M., et al. (2014). Halogenated organic pollutants in particulate matters emitted during recycling of waste printed circuit boards in a typicale-waste workshop of Southern China. *Chemosphere* 94, 143–150. doi:10.1016/j.chemosphere.2013.09.065

Rodríguez, E. A., Niño, C. J., Contreras, J. E., Vázquez-Rodríguez, F. J., López-Perales, J. F., Aguilar-Martínez, J. A., et al. (2019). Influence of incorporation of fired porcelain scrap as partial replacement of quartz on properties of an electrical porcelain. *J. Clean. Prod.* 233, 501–509. doi:10.1016/j.jclepro.2019.05.403

Romero, M., and Pérez, J. M. (2015). Relation between the microstructure and technological properties of porcelain stoneware. A review. *A Rev. Mater. construcc.*, 65, e065. doi:10.3989/mc.2015.05915

Sánchez, E., García-Ten, J., Sanz, V., and Moreno, A. (2010). Porcelain tile: almost 30 years of steady scientific-technological evolution. *Ceram. Int.* 36, 831–845. doi:10.1016/j.ceramint.2009.11.016

Sanyal, S., Kim, T., Yi, J., Koo, J.-B., Son, J.-A., and Choi, I.-H. (2020). Failure trends of high-voltage porcelain insulators depending on the constituents of the porcelain. *Appl. Sci.* 10, 694. doi:10.3390/app10020694

Sepehri, A., and Sarrafzadeh, M. H. (2018). Effect of nitrifiers community on fouling mitigation and nitrification efficiency in a membrane bioreactor. *Chem. Eng. Process. – Process Intensif.* 128, 10–18. doi:10.1016/j.cep.2018.04.006

Stathis, G., Ekonomakou, A., Stournaras, C. J., and Ftikos, C. (2004). Effect of firing conditions, filler grain size and quartz content on bending strength and physical properties of sanitaryware porcelain. *J. Eur. Ceram. Soc.* 24, 2357–2366. doi:10.1016/j.jeurceramsoc.2003.07.003

Suttibak, S., and Nitivattananon, V. (2008). Assessment of factors influencing the performance of solid waste recycling programs. *Resour. Conserv. Recycl.* 53, 45–56. doi:10.1016/j.resconrec.2008.09.004

Tam, V. W. Y., Soomro, M., and Evangelista, A. C. J. (2018). A review of recycled aggregate in concrete applications (2000–2017). *Constr. Build. Mater.* 172, 272–292. doi:10.1016/j.conbuildmat.2018.03.240

Tikul, N. (2014). Assessing environmental impact of small and medium ceramic tile manufacturing enterprises in Thailand. *J. Manuf. Syst.* 33, 1–6. doi:10.1016/j.jmsy.2013.12.002

Xie, Y., Meng, Y., Liu, S., Gong, G., Wu, Z., and Yin, Z. (2012). Fabrication and microstructure investigation of ultra-high-strength porcelain insulator. *J. Eur. Ceram. Soc.* 32, 3043–3049. doi:10.1016/j.jeurceramsoc.2012.04.015

Xu, N., Li, S., Li, Y., Xue, Z., Yuan, L., Zhang, J., et al. (2015). Preparation and properties of porous ceramic aggregates using electrical insulators waste. *Ceram. Int.* 41, 5807–5811. doi:10.1016/j.ceramint.2015.01.009